ACS APPLIED MATERIALS & INTERFACES

Research Article

www.acsami.org

Hyaluronic Acid-Modified Multifunctional Q-Graphene for Targeted Killing of Drug-Resistant Lung Cancer Cells

Yanan Luo,[†,§] Xiaoli Cai,[†] He Li,[‡] Yuehe Lin,*[,‡,§] and Dan Du*[,†,‡,§]

[†]Key Laboratory of Pesticides and Chemical Biology, Ministry of Education, College of Chemistry, Central China Normal University, Wuhan 430079, P. R. China

[‡]School of Mechanical and Materials Engineering, Washington State University, PO Box 642920 Pullman, Washington 99164, United States

[§]Paul G. Allen School for Global Animal Health, Washington State University, PO Box 647090 Pullman, Washington 99164, United States

ABSTRACT: Considering the urgent need to explore multifunctional drug delivery system for overcoming multidrug resistance, we prepared a new nanocarbon material Q-Graphene as a nanocarrier for killing drug-resistant lung cancer cells. Attributing to the introduction of hyaluronic acid and rhodamine B isothiocyanate (RBITC), the Q-Graphene-based drug delivery system was endowed with dual function of targeted drug delivery and fluorescence imaging. Additionally, doxorubicin (DOX) as a model drug was loaded on the surface of Q-Graphene via $\pi-\pi$ stacking. Interestingly, the fluorescence of DOX was quenched by Q-Graphene due to its strong electron-accepting capability, and a significant recovery of fluorescence was observed, while DOX was released from Q-Graphene. Because of the RBITC labeling and the effect of fluorescence quenching/restoring of Q-Graphene, the uptake of nanoparticles and intracellular DOX release can be tracked. Overall, a highly promising multifunctional nanoplatform was developed for tracking and monitoring targeted drug delivery for efficiently killing drug-resistant cancer cells.

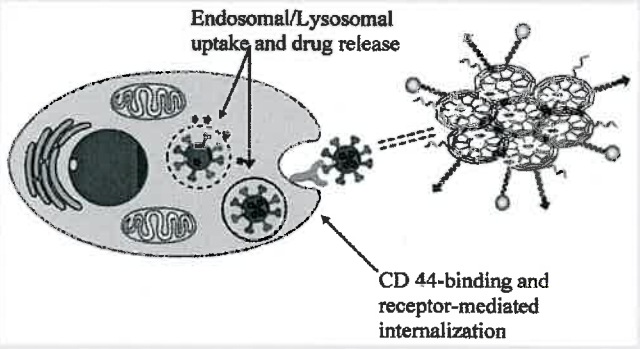

KEYWORDS: *Q-Graphene, drug delivery, MDR, tumor cell targeting, imaging*

INTRODUCTION

With the fast development of nanoscience and nanotechnology, a variety of nanoparticles have been developed as drug delivery system (DDS) due to the unique properties, such as facile synthesis, tunable size,[1] well-defined optical and surface properties, and excellent biocompatibility.[2,3] Among the inorganic nanoparticles, carbon-based nanocarriers,[4] including carbon nanotubes,[5,6] fullerenes,[7] Quantum dots,[8,9] mesoporous carbon nanospheres,[10] nanodiamonds,[11,12] graphene, and graphene derivatives[13] exhibited great superiority and potential in tumor therapy.

Two-dimensional graphene and its derivatives are some of the most promising candidates for accommodating a large amount of molecules due to their huge specific surface area. Since Liu et al.[14,15] first reported nanographene oxide as nanocarrier for DOX loading in intracellular imaging and drug delivery, graphene-based nanoplatforms had aroused extensive attention. Subsequently, Zhang's group[16] presented a dual-model drug delivery system by functionalizing graphene oxide (GO). Wang et al.[17] designed a quantum dot-conjugated graphene probe for fluorescent imaging and drug delivery. Recently, graphene and GO have been used in tumor therapy, combining chemotherapy and photothermal therapy as well as photodynamic therapy.[18−21]

Lung cancer has become one of the most deadly cancers around the world. The deficiency of lung cancer therapy is often attributed to the drug resistance of lung cancer cell and the tumor metastasis. Therefore, development of novel DDS that can overcome multidrug resistance (MDR) or tumor metastasis[22−24] will improve the efficacy of cancer therapy. Herein, hyaluronic acid (HA)-modified Q-Graphene nanoplatform was developed for targeted killing of drug-resistant lung cancer cell, which also afforded an efficient way to track and monitor the drug delivery. Q-Graphene was the latest member to join graphene family. Q-Graphene as high-volume three-dimensional spheres, which are close relatives of fullerenes, have average particle size of ~80 nm and possess a large surface area (55 m^2/g), good electrical conductivity, and outstanding thermal and chemical stabilities.[25] However, there were few reports on the biomedical applications of Q-Graphene until Banks and colleagues utilized Q-Graphene modifying electrodes as electrochemical redox probes for small molecules detection in 2012.[26] Until now, there was no report about using Q-Graphene as biomedical nanocarrier. Lung cancer cell line A549 was used as model drug-resistant tumor cell in this work. CD44 is a kind of transmembrane glycoprotein that is associated with the pathologic

Received: November 25, 2015
Accepted: January 20, 2016
Published: January 20, 2016

DOI: 10.1021/acsami.5b11471
ACS Appl. Mater. Interfaces 2016, 8, 4048−4055

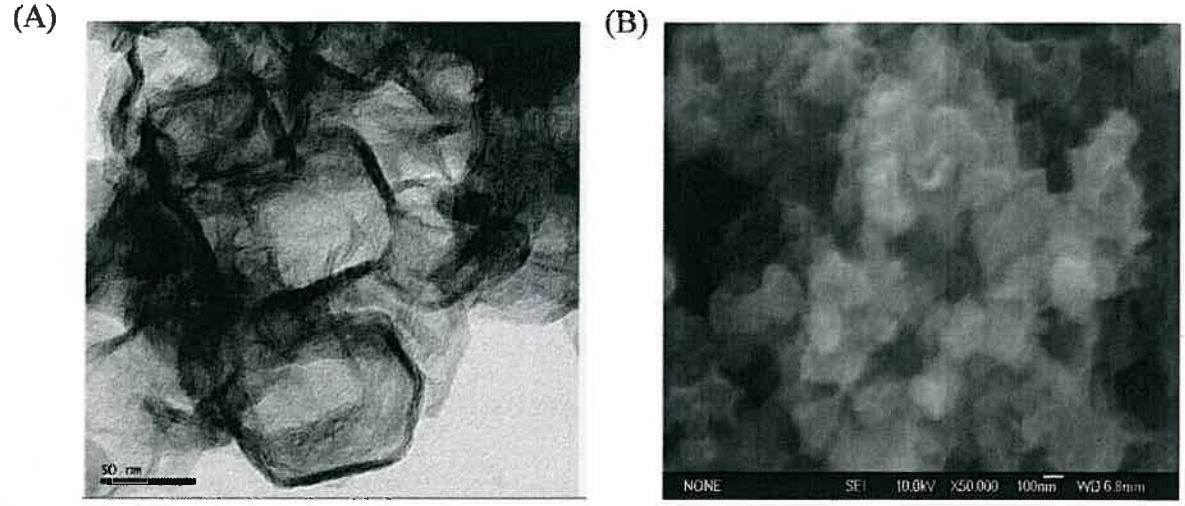

Figure 1. (A) TEM image of Q-Graphene. (B) SEM image of Q-Graphene.

activities of cancer cells and is abundantly expressed in many malignant tumors.[27,28] Because HA has a high affinity for CD44,[29] HA was conjugated to Q-Graphene by the linkage of polyoxyethylene bis(amine) (PEG) to bind CD44 that was overexpressed in A549 cells[30,31] and deliver the drug to the targeted cells via the receptor-mediated endocytosis. Further, red fluorescence dye RBITC was attached to the amine-functionalized HA-Q-Graphene to endow a fluorescent property to the nanocarrier for tracking cellular internalization of the nanoparticles. DOX was used as model drug to investigate the efficacy of the surface-modified nanoparticles toward tumor cell targeted drug delivery and release via $\pi-\pi$ stacking and hydrophobic interactions between DOX and Q-Graphene.[32−34] Unlike the fluorescence quenching of DOX, the fluorescence of RBITC was retained after conjugating to Q-Graphene because of the shield of the long carbon chain of PEG, while the DOX was absorbed on Q-Graphene directly.

EXPERIMENTAL SECTION

Chemicals and Materials. Q-Graphene (purchased from Graphene Supermarket, USA), rhodamine B isothiocyanate dye (RBITC, Sigma), PEG (Mw 2000, Aladdin), HA (Mw = 175−350 kDa, Lifecore Biomedical Co. Ltd.), doxorubicin hydrochloride (DOX, Shanghai Dibo Chemical Technology Co., Ltd.), 1-(3-(dimethylamino)propyl)-3-ethylcarbodiimide hydrochloride (EDC), sulfo-*N*-hydroxysuccinimide (NHS), 2-[*N*-morpholino] ethanesulfonic acid (MES), sulfuric acid, nitric acid, sulfanilic acid, sodium nitrite, sodium hydroxide, hydrochloric acid, fluoroboric acid, and other supplies are purchased from Sinopharm Chemical Reagent Co. Ltd., 3-(4,5-dimethylthiazol-2-yl)-2,5-diphenyltetrazolium bromide (MTT), dimethyl sulfoxide (DMSO), Dulbecco's Modified Eagle's Medium (DMEM), Minimum Essential Medium (MEM), penicillin, trypsin, and streptomycin, fetal bovine serum (FBS), phosphate buffer (PBS), 6-diamidino-2-phenylindole (DAPI), 4% formaldehyde, and other supplies are purchased from Boster Biological Technology, Ltd. Human lung epithelial tumor cell line A549 and human embryonic lung cell line MRC-5 were obtained from Type Culture Collection of the Chinese Academy of Sciences (Shanghai, China). Deionized (DI) water (18 MΩ; Millpore Co.,USA) is used throughout.

Characterization. Transmission electron microscopy (TEM) was performed at a JEOL 2011 (JEOL, Tokyo, Japan). Absorbance measurements were performed using UV-2550 UV−vis spectrophotometer (Hitachi, Japan). Fluorescence spectra are measured on Fluoro Max-P fluorescence spectrometer (HORIBA JOBIN YVON). Zeta potential experiments were performed at 25 °C using a Malvern ZetaSizer Nano instrument. X-ray photoelectron spectroscopy (XPS) analysis was performed on an ESCALAB MK II X-ray photoelectron spectrometer. Field-emission scanning electron microscopy (FE-SEM) measurements were performed using a JEOL-6700F (JEOL, Tokyo, Japan). Fourier transform infrared (FTIR) spectra were recorded in the range of 400−4000 cm^{-1} with 0.5−4 cm^{-1} resolution using a Tensor 27 FTIR spectrophotometer. Confocal laser scanning microscope (CLSM) images were observed by confocal laser scanning microscope (Nikon Ti-SH-U).

Q-Graphene Carboxylation. The carboxylic groups were grafted onto the surface of Q-Graphene following a typical experiment.[35−38] Q-Graphene (20 mg) was added into a 60 mL mixture of nitric acid/sulfuric acid (3:1 by volume, respectively). The mixture was sonicated in a bath for 8 h at ambient temperature (40 kHz with power of 950 W). Then the mixture was neutralized by 200 mL of 1 M Na_2CO_3 solution. The Q-Graphene carboxylation (Q-G-COOH) was obtained by centrifuging at 10 000 rpm for 10 min followed by rinsing with DI water several times until neutral.

Q-Graphene Sulfonation. The arenediazonium tetrafluoroborate salt was prepared according to the published literature.[39−41] Briefly, sulfanilic acid (2 g) was dissolved in 10 mL of 5 wt % sodium hydroxide solution with slight heating followed by 0.9572 g of sodium nitrite solid added into the solution. Then the mixture was cooled at 0 °C in an ice bath and added into 15.5 mL of 5 mM hydrochloric acid slowly in an ice bath under stirring, which was finished in 1 h. Subsequently, the reaction was left to proceed for another 1 h until white precipitation occurred. Then 0.74 mL of 40 wt % tetrafluoroboric acid (HBF_4) was added into the mixture under continuous vigorous stirring, and the reaction was left to proceed for 1 h. The arenediazonium tetrafluoroborate salt was obtained by vacuum filtration and rinsed with ethanol three times. Then the diazonium salt solution was added to the Q-Graphene carboxylation dispersion in an ice bath under stirring, and it was kept in ice bath for 2 h. The mixture was dialyzed against DI water for over 48 h to remove the excess diazonium salt. The obtained sulfonated Q-G-COOH was stored at 4 °C.

Synthesis of PEGylated Q-Graphene. EDC (0.2215 g) and 0.1156 g of NHS were dissolved in 1 mL of MES (pH = 6.5); then, the mixture was added to 20 mL of sulf-Q-Graphene solution. The reaction was permitted for 30 min. Subsequently, PEG, Mw 2000 was added, and the mixture was stirred for 24 h. The excess PEG was removed by dialysis against DI water for 24 h.

Conjugation of Hyaluronic Acid to Q-Graphene (HA-Q-G). HA (3 mg) was dissolved in 1.5 mL of DI water, and the pH of this solution was adjusted to 4.0 with 0.1 M HCl followed by incubation overnight. EDC (0.3 mmol) and NHS (0.3 mmol) were added, and the pH of resulting solution was adjusted to 4.0 with 0.1 M HCl and activated for 2 h at room temperature (RT). Finally, the mixture was added into 10 mL of PEGylated Q-Graphene to react on a shaker for 24 h at RT.

DOI: 10.1021/acsami.5b11471
ACS Appl. Mater. Interfaces 2016, 8, 4048−4055

Preparation of RBITC Labeled HA-Q-Graphene. RBITC was covalently linked to the residual free amine groups[5,42,43] of HA-Q-G. In brief, 1 mg of RBITC was dissolved in 1 mL of DMSO. Then 500 μL of RBITC in DMSO was mixed with 10 mL of HA-Q-G and nonHA-Q-G, respectively. The pH of the suspension was tuned to 8.0−9.0 with dilute NaOH and shaken for 24 h in dark conditions at RT. Free RBITC molecule was removed by dialysis.

Doxorubicin Loading onto the Q-Graphene. DOX was loaded onto the Q-Graphene by the following method. In brief, 2.5 mL of 1 mg/mL DOX solution was added to10 mL of RBITC-labeled Q-Graphene (HA-Q-G-RBITC and nonHA Q-G-RBITC), and the mixture was kept shaking for 24 h in dark conditions. Excess DOX was removed by dialysis. The drug loading content and entrapment efficiency were determined by the following equations:

$$\text{drug loading content}(\%) = \frac{\text{weight of drug in nanoparticles}}{\text{weight of nanoparticles taken}} \times 100$$

$$\text{drug entrapment efficiency}(\%) = \frac{\text{weight of drug in nanoparticles}}{\text{weight of drug injected}} \times 100$$

Drug Release Behaviors of HA-Q-Graphene/DOX in Vitro. In vitro release experiments were performed at pH values of 7.4 (PBS buffer) and 5.0 (acetate buffer), respectively. In detail, 1 mL of HA-Q-G-RBITC/DOX was placed in a dialysis bag with a molecular weight cutoff of 3500 Da. The dialysis bag was then immersed in 200 mL of PBS buffer or acetate buffer and kept stirring for 24 h. Samples (1 mL) were periodically collected, and each sample was replaced with the same volume of fresh buffer. The samples were analyzed with a fluorescence spectrometer to measure the amount of released DOX at an excitation wave of 485 nm.

HA-Mediated Cellular Uptake. Cellular uptake by A549 cells and MRC-5 cells were evaluated using confocal laser scanning microscopy. A549 cells and MRC-5 cells (1×10^4 cells per well) were seeded in six-well culture plates with complete DMEM and MEM, respectively, and incubated overnight. The cells were then treated with HA-Q-G-RBITC, HA-Q-G-RBITC/DOX, and Q-G-RBITC/DOX, respectively, at 37 °C for another 5 h. Then the medium was removed, and cells were washed with sterile PBS three times to remove any free material in the wells. One milliliter of 4% formaldehyde was added to each well to fix the cells at room temperature for 10 min. After the formaldehyde was removed and washed with PBS three times, DAPI (20 μL) was added to stain the cell nucleus for 3 min. Finally, the cells were washed with PBS buffer three times before capturing images by using confocal laser scanning microscope (40× oil objective). The excitation wavelengths were 405, 488, and 543 nm Nikon Ti-SH-U).

Cell Viability Assay. Cell viability analysis was performed by MTT assay. A549 cells were seeded in 96-well plate at a density of 1×10^5 cells per well and incubated for 24 h to allow the cells to attach. Cells were washed three times with PBS (pH = 7.4), and the PBS was replaced with 200 μL of fresh medium (without FBS) containing free DOX, HA-Q-G-RBITC, HA-Q-G-RBITC/DOX, or Q-G-RBITC/DOX, and then the cells were incubated in 5% CO_2 at 37 °C for 24 h. At the end of the incubation, the medium was removed. Cells were washed three times with PBS (pH = 7.4). Subsequently, 180 μL of fresh medium (without FBS) and 20 μL of MTT were added to the culture in each well, followed by incubation for 4 h. Afterward, the medium was replaced with 150 μL of DMSO to dissolve the formazan crystals. The absorbance was read at 490 nm with SpectraMax M5/M5e (Molecular Devices, USA), and the values were compared with control group.

■ RESULTS AND DISCUSSION

Preparation of HA-Q-Graphene-RBITC/DOX. In this work, Q-Graphene was selected as a suitable nanoplatform for drug delivery. The morphology of Q-Graphene, as characterized by TEM and SEM (Figure 1), showed that Q-Graphene exhibited irregularly spherical morphology. An illustration of several steps involved in preparation was revealed in Scheme 1. Q-Graphene

Scheme 1. Schematic Illustration of the Preparation of HA-Q-G-RBITC/DOX Nanoparticles and HA-Mediated Endocytosis

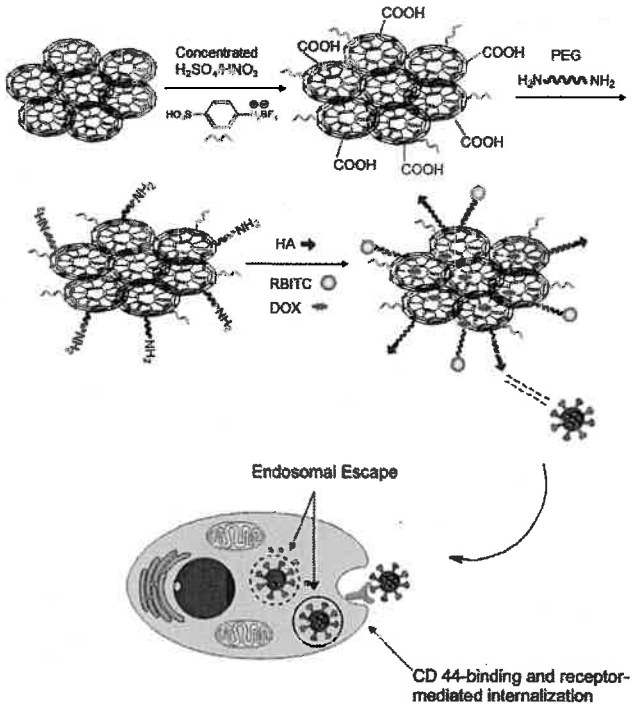

Table 1. Zeta Potential Values for the Q-Graphene Nano-functionalization

sample	Q-G-COOH	sulf-Q-G-COOH	Q-G-PEG	HA-Q-G-PEG
potential, mV	−12.7	−11.1	−1.59	−4.5

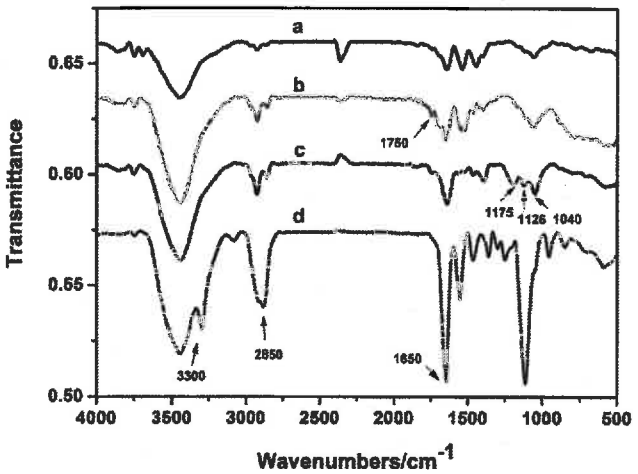

Figure 2. FTIR spectra of Q-Graphene (a), Q-Graphene-COOH (b), sulf-Q-Graphene (c), and PEG-Q-Graphene (d).

aggregates easily in aqueous solution due to its poor solubility, which was solved as follows. Q-Graphene was first grafted with carboxylic groups by the oxidation of H_2SO_4 (98 wt %) and HNO_3 (63 wt %) to increase the electrostatic repulsive force between negatively charged nanoparticles. Then, the solubility of Q-Graphene was further enhanced by the sulfonation of arenediazonium tetrafluoroborate salt. To increase stability and water dispersion of Q-Graphene and escape from the clearance

DOI: 10.1021/acsami.5b11471
ACS Appl. Mater. Interfaces 2016, 8, 4048−4055

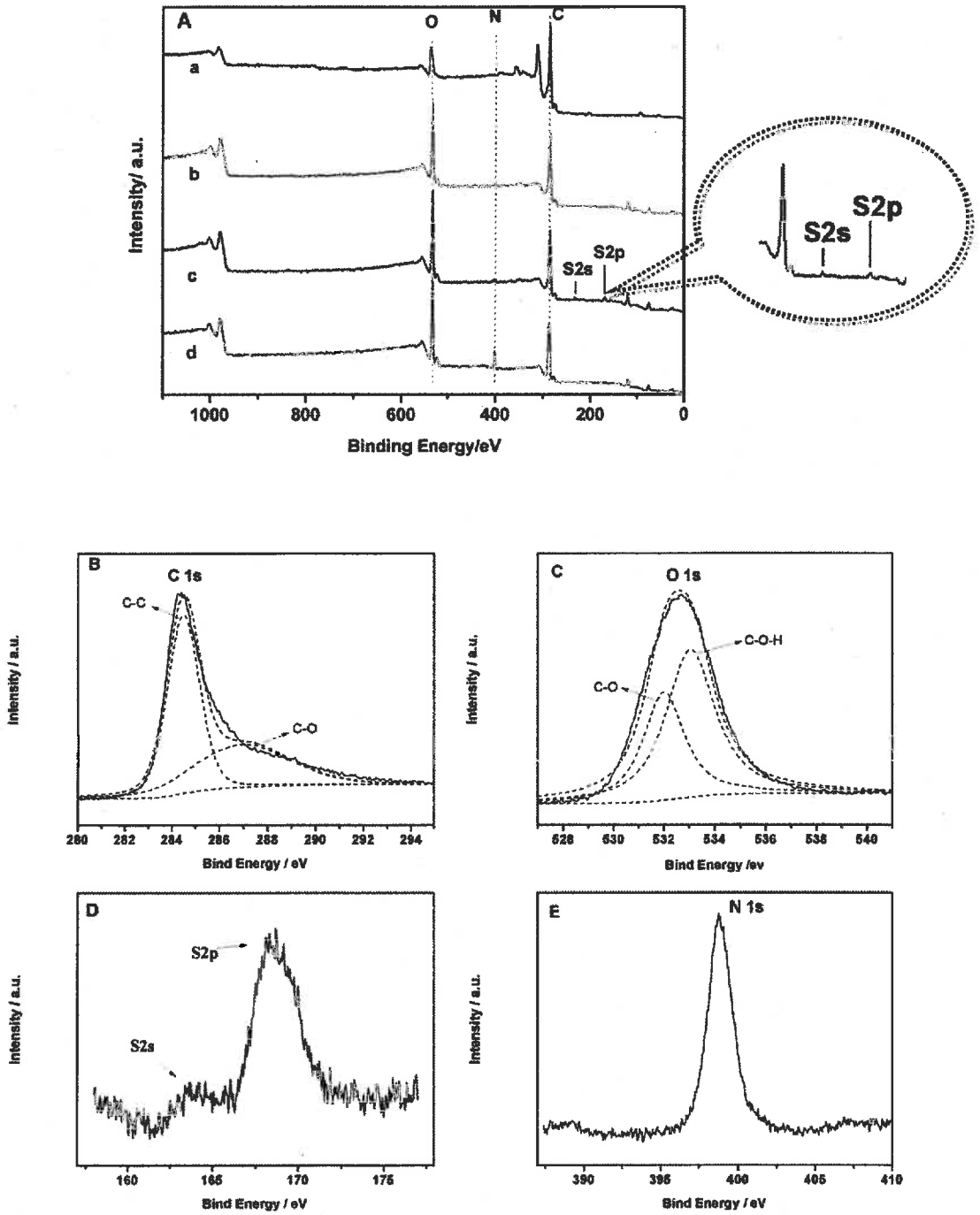

Figure 3. (A) XPS of Q-Graphene (a), Q-Graphene-COOH (b), sulf-Q-Graphene (c), PEG-Q-Graphene(d), (B) C 1s, (C) O 1s, (D) S 2s and S 2p, (E) N 1s.

of RES as well as amine functionalization, Q-Graphene was modified with polyoxyethylene bis(amine) (PEG) by amidation. Moreover, HA and RBITC were attached to Q-Graphene by the linkage of diterminal amine PEG to endow the nanoparticles with dual function of targeting and imaging. Finally, DOX was absorbed onto the Q-Graphene via $\pi-\pi$ stacking and hydrophobic interactions.

As illustrated in Table 1, Q-Graphene-COOH was endowed with a negative charge due to the presence of −COOH group on the surface. The zeta potential of Q-Graphene has a minor change after sulfonation. The value of zeta potential of Q-Graphene was changed to −1.59 mV after PEG was conjugated onto it, partly due to the introduction of amine. When further introducing HA with −COOH, the zeta potential decreased slightly.

The conversion of the modified surface of Q-Graphene was also confirmed by Fourier transform infrared (FTIR) spectra. As shown in Figure 2, the stretching vibration mode of the −COOH group was observed shifting to 1750 from 1720 cm^{-1} after Q-Graphene carboxylation (curve b). The peaks at 1040, 1126, and 1175 cm^{-1} in curve c were owing to the stretch vibration of S−O and S-phenyl, indicating the presence of sulfonic acid group. The peak emerged at 3300 cm^{-1} in curve d was due to the stretch vibration of -NH_2, indicating the PEG attached on the Q-Graphene. Simultaneously, PEGylated Q-Graphene showed

DOI: 10.1021/acsami.5b11471
ACS Appl. Mater. Interfaces 2016, 8, 4048−4055

an obvious absorption band at the pronounced stretch vibration peaks of $-CH_2$ at 2850 cm^{-1} because of the long carbon chain of PEG. The sharp absorption at 1650 cm^{-1} was due to both the $-NH_2$ bend vibration and the carbonyl−amide vibration, which was produced by amidation between carboxylic group from Q-Graphene-COOH and amine group from PEG.

Furthermore, XPS was performed to analyze the conversion of Q-Graphene according to the distinct element content.

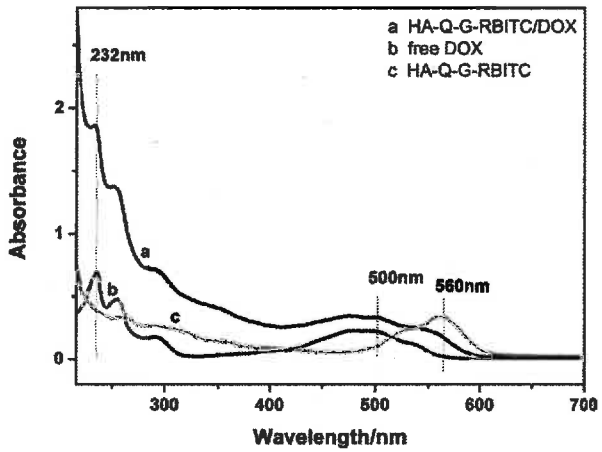

Figure 4. UV−vis absorption spectra for free DOX (b), HA-Q-G-RBITC with (a) and without (c) bound DOX.

As illustrated in Figure 3A, the oxygen content of Q-Graphene-COOH increased significantly compared to pristine Q-Graphene at 538 eV. Correspondingly, the carbon content at 284 eV decreased slightly with the oxygen content from 11.66% to 32.51%. Figure 3B,C illustrated the carbon 1s region and oxygen 1s region of original Q-Graphene. The peaks at 284.5 and 286.9 eV were attributed to C−C and C−O bonds, respectively. In Figure 3C, the peaks at 531.9 and 533.1 eV corresponded to C−O and C−O−H bonds. Consistent with IR, Q-Graphene sulfur peaks appeared at 233 and 167 eV, respectively, after sulfonation. The nitrogen peak was significantly observed at 402 eV as Q-Graphene was conjugated with PEG with $-NH_2$. The sulfur peak of Q-Graphene disappeared probably due to the presence of nitrogen, which led to the relative content of sulfur decreasing.

Drug Loading and Release in Vitro. Figure 4 illustrated UV−vis spectra of HA-Q-G-RBITC, free DOX, and HA-Q-G-RBITC/DOX. The loading content and entrapment efficiency of DOX in HA-Q-G-RBITC are found to be 30% and 86%, respectively. There was no significant absorption observed in the range of 200−500 nm but a peak at 560 nm, which came from RBITC of HA-Q-G-RBITC (curve c). Free DOX displays absorption at 232, 255, and 490 nm (curve b), and the peak was slightly red-shifted from 490 to 500 nm after DOX adsorbed on the surface of Q-Graphene (curve a), indicating DOX loaded on Q-Graphene.

HA-Q-G was promoted to fluorescent platform with the red fluorescence dye RBITC to track intracellular distribution of

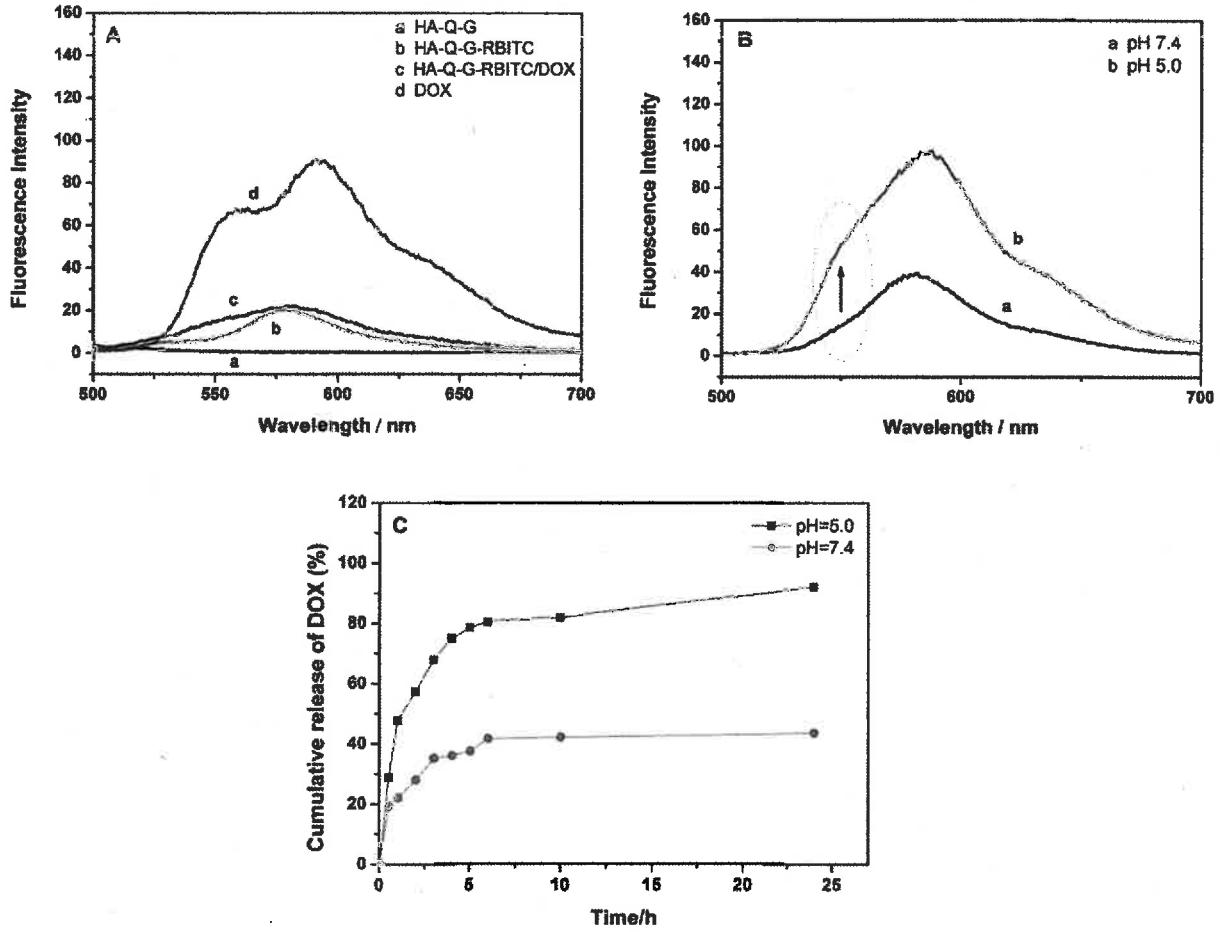

Figure 5. (A) Fluorescence emission spectra of HA-Q-G (a), HA-Q-G-RBITC (b), HA-Q-G-RBITC/DOX (c), and free DOX (d). (B) Fluorescence emission spectra for HA-Q-G-RBITC/DOX in pH 5.0 acetate buffer (b) and pH 7.4 PBS (a). (C) DOX release profile from the HA-Q-G-RBITC/DOX complexes at RT in pH 5.0 acetate buffer (black curve) and pH 7.4 PBS (red curve).

DOI: 10.1021/acsami.5b11471
ACS Appl. Mater. Interfaces 2016, 8, 4048−4055

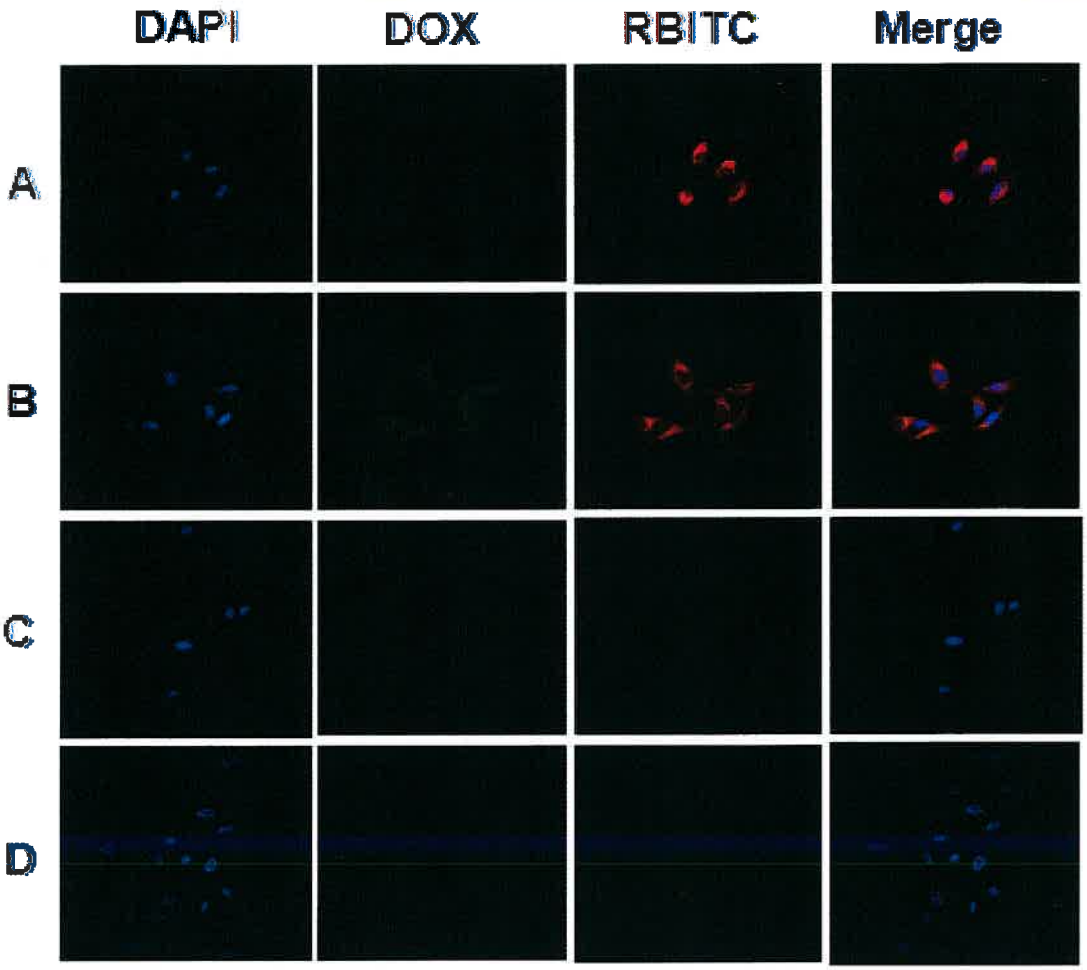

Figure 6. CLSM images of A549 cells incubated with (A) HA-Q-G-RBITC, (B) HA-Q-G-RBITC/DOX, (C) Q-G-RBITC/DOX for 5 h. (D) MRC-5 cells incubated with HA-Q-G-RBITC/DOX for 5 h.

nanoparticles. As shown in Figure 5A, HA-Q-G-RBITC showed emission at 578 nm at excitation 485 nm (curve b), while HA-Q-G showed no emission at the same position (curve a). However, the fluorescence of DOX was quenched once attached onto Q-Graphene (curve c). Figure 5B shows a fluorescence recovery of DOX after releasing from Q-Graphene incubated with pH 5.0 acetate buffer (curve b) for 4 h, while a fluorescence quenching was found in pH 7.4 PBS (curve a). The emission at 585 nm of pH 7.4 PBS was attributed to the fluorescence of RBITC. An acid-pH-triggered drug release mechanism was hypothesized reasonably in this Q-Graphene-based DDS, which was attributed to the protonation of DOX and enhanced hydrophilicity at acidic condition. The DOX release curve of DOX from Q-Graphene in vitro was shown in Figure 5C; the release amount of DOX constantly increased with release time. A rapid increase of DOX releasing was observed in both pH 5.0 acetate buffer and pH 7.4 PBS in first 6 h. At the point of 24 h, the release amount of DOX sustainably increased to ~85% in pH 5.0 acetate buffer, while it reached platform ~42% at 10 h in pH 7.4 PBS.

Fluorescence Imaging and Cellular Uptake. The selectivity of HA-Q-G-RBITC against glycoprotein CD44 was investigated in Figure 6. To verify the specific targeting ability of HA in the cellular uptake of Q-Graphene-based delivery system, human lung epithelial tumor cell line A549 with CD44 high expression and human embryonic lung cell line MRC-5 with CD44 low expression were used as models. A549 cells were incubated with HA-Q-G-RBITC/DOX and Q-G-RBITC/DOX, respectively, at a concentration of DOX at 8 $\mu g \cdot mL^{-1}$ for 5 h. Additionally, HA negative MRC-5 cells incubation with HA-Q-G-RBITC/DOX as negative control experiment was used for comparison. The DOX emits green fluorescence under irradiation with blue light, while the dye RBITC emits red fluorescence under green light excitation. The differential fluorescence of DOX and RBITC was utilized to track the uptake process of Q-Graphene/DOX and intracellular DOX releasing. Figure 6A exhibited a strong red signal from RBITC in cytoplasm, indicating the RBITC-labeled HA-Q-G sufficiently internalized by A549 cells. No significant red signal was found in the nucleus, which indicated HA-Q-G-RBITC unable transporting across the nuclear membrane postcellular uptake. However, A549 cells showed both bright green fluorescence and red fluorescence when incubated with Q-G-RBITC/DOX (Figure 6B). The bright green fluorescence almost filled cells including cytoplasmic and nucleus area, indicating the DOX releasing from Q-Graphene and penetrating into the nucleus to induce cell apoptosis. Compared with A549 cells incubated with HA-Q-G-RBITC/DOX, Figure 6C showed weaker green and red fluorescences. It was attributed to the high affinity of HA to CD44 that was overexpressed by A549 cells. In absence of HA, only rare Q-G-RBITC/DOX could be internalized by pagocytosis and pinocytosis instead of through the receptor-mediated endocytosis. Moreover, MRC-5 cells incubated with HA-Q-G-RBITC/DOX (Figure 6D) displayed

DOI: 10.1021/acsami.5b11471
ACS Appl. Mater. Interfaces 2016, 8, 4048−4055

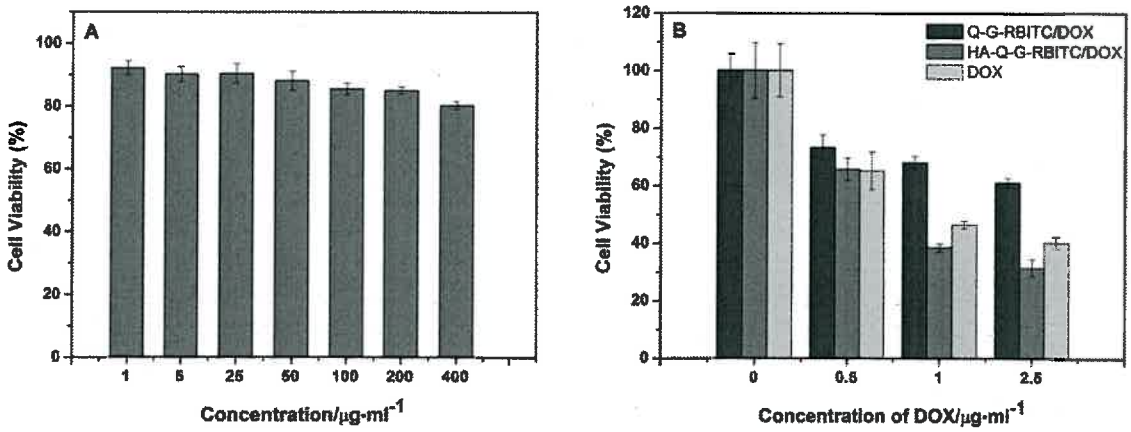

Figure 7. (A) In vitro cytotoxic effects of HA-Q-G-RBITC against A549 cells at different nanoparticles concentration. (B) Cytotoxic effects of Q-G-RBITC/DOX, HA-Q-G-RBITC/DOX, and DOX against A549 cells with increasing DOX concentration.

pale fluorescence in cytoplasm due to CD44 negatively expressed on the cell membrane. It was evident that HA played a crucial role in specifically targeting tumor cells.

In Vitro Cytotoxicity Assay. To evaluate the biosafety of Q-Graphene-based drug delivery system, the in vitro cytotoxicity of RBITC labeled HA-Q-G against A549 cells was assessed using MTT assay. Figure 7A showed the cytotoxicity of HA-Q-G-RBITC nanoparticles at different concentrations (1, 5, 25, 50, 100, 200, and 400 $\mu g \cdot mL^{-1}$). No significant cytotoxicity was observed after incubation with HA-Q-G-RBITC for 48 h, even when the concentration was as high as 400 $\mu g \cdot mL^{-1}$, which implied that HA-Q-G-RBITC could be taken as a safe drug nanocarrier. The cytotoxicity of HA-Q-G-RBITC to human embryonic lung cell line MRC-5 cells was tested, and no significant cytotoxicity was observed in the concentration range of 0–200 $\mu g \cdot mL^{-1}$ (not shown in the text). Considering the low cytotoxicity of HA-Q-G-RBITC, the killing effect of HA-Q-G-RBITC/DOX against A549 cells was measured. A549 cells were incubated with HA-Q-G-RBITC/DOX, Q-G-RBITC/DOX, and free DOX, respectively, at different concentrations for 48 h. As shown in Figure 7B, the cell viability decreased with the increasing concentration of DOX for each group. More than half of the cells were killed when the DOX was 1 $\mu g \cdot mL^{-1}$ of HA-Q-G-RBITC/DOX and free DOX, but more than 70% cells survived when the DOX was 2.5 $\mu g \cdot mL^{-1}$ of Q-G-RBITC/DOX. That may be explained by the special affinity of HA to CD44 on the cells inducing higher internalization efficiency by A549 cells. When DOX concentration increased from 1 to 2.5 $\mu g \cdot mL^{-1}$, only minor cytotoxicity increased with only DOX treatment. This can be attributed to the drug resistance effect from P-glycoprotein driving drug efflux. Increasing drug efflux pumps on the cell membrane is one of the main mechanisms by which cells become MDR. By loading drugs on nanoparticles that bypass the efflux pumps, the intracellular concentration of the drug was hence increased. In comparison, HA-Q-G-RBITC/DOX showed higher cytotoxicity than free DOX when DOX loading concentration was above 1 $\mu g \cdot mL^{-1}$. HA-Q-G-RBITC/DOX exhibited lower IC_{50} value (0.8651 $\mu g \cdot mL^{-1}$) than free DOX (1.1302 $\mu g \cdot mL^{-1}$) against A549 cells, indicating the developed HA-Q-G-RBITC/DOX are capable of efficiently killing drug-resistant cancer cells.

■ CONCLUSION

In summary, we have designed a dual-fluorescence imaging probe upon Q-Graphene-based nanoplatform for efficiently killing MDR cancer cells. Coupled with targeting ligands HA, Q-Graphene was endowed with effectively targeting tumor cells. In this DDS, the nanoparticles were effectively internalized by HA-positive A549 cells through HA-mediated cellular endocytosis, which allowed the HA-Q-G-RBITC as an excellent drug delivery nanoplatform. In addition, the detachment of DOX from Q-Graphene into the cancer cell nuclei by acidically triggering alleviated the side effect of DOX on the normal cells due to the absence of intracellular acidic environment in normal cells. This DDS exhibited high efficiency in targeted drug delivery to cancer cells and has a great potential for killing drug-resistant cancer cells.

■ AUTHOR INFORMATION

Corresponding Authors

*E-mail: dan.du@mail.ccnu.edu.cn. (D.D.)
*E-mail: yuehe.lin@wsu.edu. (Y.L.)

Notes

The authors declare no competing financial interest.

■ ACKNOWLEDGMENTS

This work was partly supported by the National Natural Science Foundation of China (21575047, 21275062). D.D. and Y.L. acknowledge the Centers for Disease Control and Prevention/National Institute for Occupational Safety and Health (CDC/NIOSH) Grant No. R21OH010768. Its contents are solely the responsibility of the authors and do not necessary represent the official views of CDC. We acknowledge Ms. Y. Yang in Wuhan Institute of Physics and Mathematics, Chinese Academy of Sciences, for confocal imaging support.

■ REFERENCES

(1) Valtchev, V.; Tosheva, L. Porous Nanosized Particles: Preparation, Properties, and Applications. *Chem. Rev.* **2013**, *113*, 6734–6760.
(2) Lee, S.-M.; Nguyen, S. T. Smart Nanoscale Drug Delivery Platforms from Stimuli-Responsive Polymers and Liposomes. *Macromolecules* **2013**, *46*, 9169–9180.
(3) Adair, J. H.; Parette, M. P.; Altinoglu, E. I.; Kester, M. Nanoparticulate Alternatives for Drug Delivery. *ACS Nano* **2010**, *4*, 4967–4970.
(4) Lim, D. J.; Sim, M.; Oh, L.; Lim, K.; Park, H. Carbon-Based Drug Delivery Carriers for Cancer Therapy. *Arch. Pharmacal Res.* **2014**, *37*, 43–52.
(5) Cheng, J.; Fernando, K. A.; Veca, L. M.; Sun, Y. P.; Lamond, A. I.; Lam, Y. W.; Cheng, S. H. Reversible Accumulation of PEGylated Single-

DOI: 10.1021/acsami.5b11471
ACS Appl. Mater. Interfaces 2016, 8, 4048–4055

walled Carbon Nanotubes in the Mammalian Nucleus. *ACS Nano* **2008**, *2*, 2085−2094.
(6) Wu, H.; Shi, H.; Zhang, H.; Wang, X.; Yang, Y.; Yu, C.; Hao, C.; Du, J.; Hu, H.; Yang, S. Prostate Stem Cell Antigen Antibody-Conjugated Multiwalled Carbon Nanotubes for Targeted Ultrasound Imaging and Drug Delivery. *Biomaterials* **2014**, *35*, 5369−5380.
(7) Fan, J.; Fang, G.; Zeng, F.; Wang, X.; Wu, S. Water-Dispersible Fullerene Aggregates as a Targeted Anticancer Prodrug with both Chemo- and Photodynamic Therapeutic Actions. *Small* **2013**, *9*, 613−621.
(8) Zhang, X.; Wang, S.; Zhu, C.; Liu, M.; Ji, Y.; Feng, L.; Tao, L.; Wei, Y. Carbon-Dots Derived from Nanodiamond: Photoluminescence Tunable Nanoparticles for Cell Imaging. *J. Colloid Interface Sci.* **2013**, *397*, 39−44.
(9) Bharali, D. J.; Lucey, D. W.; Jayakumar, H.; Pudavar, H. E.; Prasad, P. N. Folate-Receptor-Mediated Delivery of InP Quantum Dots for Bioimaging Using Confocal and Two-Photon Microscopy. *J. Am. Chem. Soc.* **2005**, *127*, 11364−11371.
(10) Zhu, J.; Liao, L.; Zhu, L.; Kong, J.; Liu, B. Folate Functionalized Mesoporous Carbon Nanospheres as Nanocarrier for Targetted Delivery and Controlled Release of Doxorubicin to Hela Cells. *Huaxue Xuebao* **2013**, *71*, 69−74.
(11) Zhang, Z.; Niu, B.; Chen, J.; He, X.; Bao, X.; Zhu, J.; Yu, H.; Li, Y. The Use of Lipid-Coated Nanodiamond to Improve Bioavailability and Efficacy of Sorafenib in Resisting Metastasis of Gastric Cancer. *Biomaterials* **2014**, *35*, 4565−4572.
(12) Mochalin, V. N.; Shenderova, O.; Ho, D.; Gogotsi, Y. The Properties and Applications of Nanodiamonds. *Nat. Nanotechnol.* **2011**, *7*, 11−23.
(13) Yang, Y.; Asiri, A. M.; Tang, Z.; Du, D.; Lin, Y. Graphene Based Materials for Biomedical Applications. *Mater. Today* **2013**, *16*, 365−373.
(14) Liu, Z.; Robinson, J. T.; Sun, X.; Dai, H. PEGylated Nanographene Oxide for Delivery of Water-Insoluble Cancer Drugs. *J. Am. Chem. Soc.* **2008**, *130*, 10876−10877.
(15) Sun, X.; Liu, Z.; Welsher, K.; Robinson, J. T.; Goodwin, A.; Zaric, S.; Dai, H. Nano-Graphene Oxide for Cellular Imaging and Drug Delivery. *Nano Res.* **2008**, *1*, 203−212.
(16) Zhang, L.; Xia, J.; Zhao, Q.; Liu, L.; Zhang, Z. Functional Graphene Oxide as a Nanocarrier for Controlled Loading and Targeted Delivery of Mixed Anticancer Drugs. *Small* **2010**, *6*, 537−544.
(17) Chen, M. L.; He, Y. J.; Chen, X. W.; Wang, J. H. Quantum-Dot-Conjugated Graphene as a Probe for Simultaneous Cancer-Targeted Fluorescent Imaging, Tracking, and Monitoring Drug Delivery. *Bioconjugate Chem.* **2013**, *24*, 387−397.
(18) Yang, K.; Zhang, S.; Zhang, G.; Sun, X.; Lee, S. T.; Liu, Z. Graphene in Mice: Ultrahigh *in vivo* Tumor Uptake and Efficient Photothermal Therapy. *Nano Lett.* **2010**, *10*, 3318−3323.
(19) Kim, H.; Lee, D.; Kim, J.; Kim, T. I.; Kim, W. J. Photothermally Triggered Cytosolic Drug Delivery Via Endosome Disruption Using a Functionalized Reduced Graphene Oxide. *ACS Nano* **2013**, *7*, 6735−6746.
(20) Zhou, L.; Wang, W.; Tang, J.; Zhou, J. H.; Jiang, H. J.; Shen, J. Graphene Oxide Noncovalent Photosensitizer and Its Anticancer Activity *in vitro*. *Chem. - Eur. J.* **2011**, *17*, 12084−12091.
(21) Tian, B.; Wang, C.; Zhang, S.; Feng, L.; Liu, Z. Photothermally Enhanced Photodynamic Therapy Delivered by Nano-Graphene Oxide. *ACS Nano* **2011**, *5*, 7000−7009.
(22) Creixell, M.; Peppas, N. A. Co-Delivery of SiRNA and Therapeutic Agents Using Nanocarriers to Overcome Cancer Resistance. *Nano Today* **2012**, *7*, 367−369.
(23) Zhou, J.; Zhao, W. Y.; Ma, X.; Ju, R. J.; Li, X. Y.; Li, N.; Sun, M. G.; Shi, J. F.; Zhang, C. X.; Lu, W. L. The Anticancer Efficacy of Paclitaxel Liposomes Modified with Mitochondrial Targeting Conjugate in Resistant Lung Cancer. *Biomaterials* **2013**, *34*, 3626−3638.
(24) Long, J. T.; Cheang, T. Y.; Zhuo, S. Y.; Zeng, R. F.; Dai, Q. S.; Li, H. P.; Fang, S. Anticancer Drug-Loaded Multifunctional Nanoparticles to Enhance the Chemotherapeutic Efficacy in Lung Cancer Metastasis. *J. Nanobiotechnol.* **2014**, *12*, 37.
(25) http://emuch.net/html/201106/3327416.html.
(26) Randviir, E. P.; Brownson, D. A.; Gomez-Mingot, M.; Kampouris, D. K.; Iniesta, J.; Banks, C. E. Electrochemistry of Q-Graphene. *Nanoscale* **2012**, *4*, 6470−6480.
(27) Qhattal, H. S.; Liu, X. Characterization of CD44-Mediated Cancer Cell Uptake and Intracellular Distribution of Hyaluronan-Grafted Liposomes. *Mol. Pharmaceutics* **2011**, *8*, 1233−1246.
(28) Zöller, M. CD44: Can a Cancer-Initiating Cell Profit From an Abundantly Expressed Molecule? *Nat. Rev. Cancer* **2011**, *11*, 254−267.
(29) Hu, K.; Zhou, H.; Liu, Y.; Liu, Z.; Liu, J.; Tang, J.; Li, J.; Zhang, J.; Sheng, W.; Zhao, Y.; Wu, Y.; Chen, C. Hyaluronic Acid Functional Amphipathic and Redox-Responsive Polymer Particles for the Co-Delivery of Doxorubicin and Cyclopamine to Eradicate Breast Cancer Cells and Cancer Stem Cells. *Nanoscale* **2015**, *7*, 8607−8618.
(30) Hyung, W.; Ko, H.; Park, J.; Lim, E.; Park, S. B.; Park, Y. J.; Yoon, H. G.; Suh, J. S.; Haam, S.; Huh, Y. M. Novel Hyaluronic Acid (HA) Coated Drug Carriers (HCDCs) for Human Breast Cancer Treatment. *Biotechnol. Bioeng.* **2008**, *99*, 442−454.
(31) Li, F.; Park, S.-J.; Ling, D.; Park, W.; Han, J. Y.; Na, K.; Char, K. Hyaluronic Acid-Conjugated Graphene Oxide/Photosensitizer Nanohybrids for Cancer Targeted Photodynamic Therapy. *J. Mater. Chem. B* **2013**, *1*, 1678−1686.
(32) Liu, G.; Shen, H.; Mao, J.; Zhang, L.; Jiang, Z.; Sun, T.; Lan, Q.; Zhang, Z. Transferrin Modified Graphene Oxide for Glioma-Targeted Drug Delivery: *in vitro* and *in vivo* Evaluations. *ACS Appl. Mater. Interfaces* **2013**, *5*, 6909−6914.
(33) Pan, Y.; Bao, H.; Sahoo, N. G.; Wu, T.; Li, L. Water-Soluble Poly(N-isopropylacrylamide)-Graphene Sheets Synthesized via Click Chemistry for Drug Delivery. *Adv. Funct. Mater.* **2011**, *21*, 2754−2763.
(34) Bao, H.; Pan, Y.; Ping, Y.; Sahoo, N. G.; Wu, T.; Li, L.; Li, J.; Gan, L. H. Chitosan-Functionalized Graphene Oxide as a Nanocarrier for Drug and Gene Delivery. *Small* **2011**, *7*, 1569−1578.
(35) Tang, D.; Tang, J.; Su, B.; Chen, G. Ultrasensitive Electrochemical Immunoassay of Staphylococcal Enterotoxin B in Food Using Enzyme-Nanosilica-Doped Carbon Nanotubes for Signal Amplification. *J. Agric. Food Chem.* **2010**, *58*, 10824−10830.
(36) Zhang, J.; Zou, H.; Qing, Q.; Yang, Y.; Li, Q.; Liu, Z.; Guo, X.; Du, Z. Effect of Chemical Oxidation on the Structure of Single-Walled Carbon Nanotubes. *J. Phys. Chem. B* **2003**, *107*, 3712−3718.
(37) Goyanes, S.; Rubiolo, G. R.; Salazar, A.; Jimeno, A.; Corcuera, M. A.; Mondragon, I. Carboxylation Treatment of Multiwalled Carbon Nanotubes Monitored by Infrared and Ultraviolet Spectroscopies and Scanning Probe Microscopy. *Diamond Relat. Mater.* **2007**, *16*, 412−417.
(38) Eitan, A.; Jiang, K.; Dukes, D.; Andrews, R.; Schadler, L. S. Surface Modification of Multiwalled Carbon Nanotubes: Toward the Tailoring of the Interface in Polymer Composites. *Chem. Mater.* **2003**, *15*, 3198−3201.
(39) Zhu, Y.; Tour, J. M. Graphene Nanoribbon Thin Films Using Layer-by-Layer Assembly. *Nano Lett.* **2010**, *10*, 4356−4362.
(40) Huang, P.; Xu, C.; Lin, J.; Wang, C.; Wang, X.; Zhang, C.; Zhou, X.; Guo, S.; Cui, D. Folic Acid-Conjugated Graphene Oxide Loaded with Photosensitizers for Targeting Photodynamic Therapy. *Theranostics* **2011**, *1*, 240−50.
(41) Si, Y.; Samulski, E. T. Synthesis of Water Soluble Graphene. *Nano Lett.* **2008**, *8*, 1679−1682.
(42) Sahoo, B.; Devi, K. S.; Banerjee, R.; Maiti, T. K.; Pramanik, P.; Dhara, D. Thermal and pH Responsive Polymer-Tethered Multifunctional Magnetic Nanoparticles for Targeted Delivery of Anticancer Drug. *ACS Appl. Mater. Interfaces* **2013**, *5*, 3884−3893.
(43) Gu, Y. J.; Cheng, J.; Lin, C. C.; Lam, Y. W.; Cheng, S. H.; Wong, W. T. Nuclear Penetration of Surface Functionalized Gold Nanoparticles. *Toxicol. Appl. Pharmacol.* **2009**, *237*, 196−204.

DOI: 10.1021/acsami.5b11471
ACS Appl. Mater. Interfaces 2016, 8, 4048−4055